Nonlinear Analysis: Modelling and Control, 2010, Vol. 15, No. 2, 139–154

Unsteady natural convective power-law fluid flow past a vertical plate embedded in a non-Darcian porous medium in the presence of a homogeneous chemical reaction

A.J. Chamkha[1], **A.M. Aly**[2], **M.A. Mansour**[3]

[1]Manufacturing Engineering Department
The Public Authority for Applied Education and Training
Shuweikh 70654, Kuwait
achamkha@yahoo.com

[2]Department of Mathematics, Faculty of Science, South Valley University
Qena, Egypt

[3]Department of Mathematics, Faculty of Science, Assuit University
Assuit, Egypt

Received: 2009-03-15 **Revised:** 2009-11-07 **Published online:** 2010-06-01

Abstract. A numerical solution is presented for unsteady coupled heat and mass transfer by natural convection from a non-Newtonian power-law fluid flow past a vertical plate embedded in a non-Darcian porous medium in the presence of viscous dissipation and chemical reaction effects. The governing equations are formulated and a numerical solution is obtained by using an explicit finite-difference scheme. The solutions at each time step have been found to reach the steady state solution properly. The numerical results are presented in tabular and graphical form to show the effects of material parameters of the problem on the solution.

Keywords: finite-difference solution, non-Newtonian fluid, unsteady flow, chemical reaction, porous medium.

1 Introduction

Natural convection in a fluid-saturated porous medium is of fundamental importance in many industrial and environmental problems. Moreover, heat and mass transfer from a vertical flat plate is encountered in various applications such as heat exchangers, cooling systems and electronic equipment. In addition, Non-Newtonian fluids such as molten plastics, polymers, glues, ink, pulps, foodstuffs or slurries are increasingly used in various manufacturing, industrial and engineering applications especially in the chemical engineering processes.

In general, chemical reactions in mass transfer problems include two types. A homogeneous chemical reaction is one that occurs uniformly throughout a given phase. The

species generation in a homogeneous reaction is analogous to internal source of heat generation. In contrast, a heterogeneous reaction takes place in a restricted region or within the boundary of a phase. It can therefore be treated as a boundary condition similar to the constant heat flux condition in heat transfer.

The study of heat and mass transfer with a chemical reaction is of great practical importance to engineers and scientists because of its almost universal occurrence in many branches of science and engineering [1]. Kandasamy et al. [1] have studies the effects of chemical reaction and heat and mass transfer on MHD flow over a vertical stretching surface with heat source and thermal stratification. In the past decades, the penetration theory of Highie 1935 had been widely applied to unsteady state diffusion problems with and without chemical reaction. As far as one can ascertain, all the solutions with chemical reaction were obtained for the case of a semi-infinite body of liquid, although physical absorption into a finite film was considered. Among some of the interesting problems which were studied is the analysis of laminar forced convection mass transfer with homogeneous chemical reaction [2]. The effect of different values of Prandtl number of the fluid along the surface has been analyzed and reported by Gebhart [3]. The effects of mass transfer on flow past an impulsively started infinite vertical plate with constant heat flux and chemical reaction have been studied by Das et al. [4]. Andersson et al. [5] have studied the flow and mass diffusion of a chemical species with first-order and higher-order reactions over a linearly stretching surface.

All the above referenced studies have dealt with flows of Newtonian fluids. In recent years, non-Newtonian liquids have been appearing in increasing numbers. In spite of the extensive research over the past few decades which dealt with the flow of non-Newtonian fluids, there has been little work done on the unsteady flow for non-Newtonian fluids. Abd El-Naby et al. [6] have analyzed the effect of radiation on MHD unsteady free-convection flow past a semi-infinite vertical porous plate. Ganesan and Palani [7] have studied unsteady natural convection MHD flow past an inclined plate with variable surface heat and mass flux. El-Kabeir et al. [8] have considered unsteady MHD combined convection over a moving vertical sheet in a fluid saturated porous medium with uniform surface heat flux. Mbeledogu and Ogulu [9] have considered heat and mass transfer of an unsteady MHD natural convection flow of a rotating fluid past a vertical porous flat plate in the presence of radiative heat transfer. Usha and Sridharan [10] have reported on the motion of a liquid film on an unsteady stretching surface. Andersson et al. [11] have studied heat transfer in a liquid film on an unsteady stretching surface. Also, Andersson et al. [12] have analyzed flow of a power-law fluid film on an unsteady stretching surface. Chen [13] has considered heat transfer in a power-law fluid film over a unsteady stretching sheet.

Very recently, Amir and Kayvan [14] have used the homotopy analysis method for solving unsteady MHD flow of Maxwellian fluids above impulsively stretching sheets. Bég et al. [15] have employed Network numerical simulator for time-dependent nonlinear buoyancy-driven double-diffusive radiative convection flow in non-Darcy geological porous media. In the present work, a numerical solution is presented for unsteady coupled heat and mass transfer by natural convection from a non-Newtonian power-law fluid flow past a vertical plate embedded in a porous medium in the presence of viscous dissipation

and chemical reaction effects.

2 Mathematical analysis

Many different types of non-Newtonian fluids exist but the simplest and most common type is the power-law fluid for which the theological equation of state between stress components and strain rate components defined by Vujanovic et al. [16] is

$$\tau_{i,j} = -P\delta_{i,j} + K\left|\sum_{m=1}^{3}\sum_{I=1}^{3} e_{Im}e_{Im}\right|^{(n-1)/2} e_{i,j}, \tag{1}$$

where P is the pressure, $\delta_{i,j}$ is the Kronecker delta, and K and n are the consistency and flow behavior indices of the fluid. When $n > 1$ the fluid is described as dilatant, $n < 1$ as pseudo-plastic and when $n = 1$ it is known as the Newtonian fluid.

Consider unsteady, laminar, boundary-layer, two-dimensional free convective flow of a non-Newtonian power-law fluid over a vertical flat plate embedded in a non-Darcian porous medium in the presence of viscous dissipation effects. The fluid properties are assumed to be constant and a first-order homogeneous chemical reaction is assumed to take place in the flow. Under these assumptions with the usual Boussinesq approximation, the governing boundary-layer equations that are based on the balance laws of mass, linear momentum, energy and concentration species for this investigation can be written as:

$$\frac{\partial \bar{u}}{\partial \bar{x}} + \frac{\partial \bar{v}}{\partial \bar{y}} = 0, \tag{2}$$

$$\frac{\partial \bar{u}}{\partial \bar{t}} + \bar{u}\frac{\partial \bar{u}}{\partial \bar{x}} + \bar{v}\frac{\partial \bar{u}}{\partial \bar{y}} = \frac{k}{\rho}\frac{\partial}{\partial \bar{y}}\left(\left|\frac{\partial \bar{u}}{\partial \bar{y}}\right|^{n-1}\frac{\partial \bar{u}}{\partial \bar{y}}\right) + g\beta_T\left(\bar{T} - \bar{T}_\infty\right) + g\beta_C\left(\bar{C} - \bar{C}_\infty\right) - \frac{k\varepsilon^n}{\rho k_1}|\bar{u}|^{n-1}\bar{u} - \frac{F\varepsilon^2}{k_1^{1/2}}|\bar{u}|\bar{u}, \tag{3}$$

$$\frac{\partial \bar{T}}{\partial \bar{t}} + \bar{u}\frac{\partial \bar{T}}{\partial \bar{x}} + \bar{v}\frac{\partial \bar{T}}{\partial \bar{y}} = \alpha\frac{\partial^2 \bar{T}}{\partial \bar{y}^2} + \frac{k}{\rho C_p}\left(\left|\frac{\partial \bar{u}}{\partial \bar{y}}\right|^{n-1}\frac{\partial \bar{u}}{\partial \bar{y}}\right), \tag{4}$$

$$\frac{\partial \bar{C}}{\partial \bar{t}} + \bar{u}\frac{\partial \bar{C}}{\partial \bar{x}} + \bar{v}\frac{\partial \bar{C}}{\partial \bar{y}} = D\frac{\partial^2 \bar{C}}{\partial \bar{y}^2} - k_c\left(\bar{C} - \bar{C}_\infty\right), \tag{5}$$

where $\bar{x}$ and $\bar{y}$ are the Cartesian coordinates and $\bar{t}$ represents time. $\bar{u}$ and $\bar{v}$ are the velocity components along $\bar{x}$ and $\bar{y}$ axis. ρ is the fluid density, k is the thermal conductivity, C_p is the specific heat at constant pressure and $\nu = \mu/\rho$ is the kinematic viscosity, where μ is the constant viscosity of the fluid in the boundary layer region, k_c is the rate of chemical reaction, g is the acceleration due to gravity, β_T is the volumetric coefficient of thermal expansion, β_C is the volumetric coefficient of concentration expansion. k_1, ε and F are the permeability of porous media, porosity and the empirical constant, respectively, D_m is the coefficient of mass diffusivity $\bar{T}_\infty$ and $\bar{C}_\infty$ are the free stream temperature and concentration, respectively.

The initial and boundary conditions are:

$$\begin{aligned}
&\bar{t}=0: \quad \bar{u}=\bar{v}=0, \ \bar{T}=\bar{T}_\infty, \ \bar{C}=\bar{C}_\infty \quad \text{for all } \bar{x} \text{ and } \bar{y},\\
&\bar{t}>0: \quad \bar{u}=\bar{v}=0, \ \bar{T}=\bar{T}_\infty, \ \bar{C}=\bar{C}_\infty \quad \text{at } \bar{x}=0,\\
&\qquad\quad \bar{u}=\bar{v}=0, \ \bar{T}=\bar{T}_w, \ \bar{C}=\bar{C}_w \quad \text{at } \bar{y}=0, \ \bar{x}>0,\\
&\qquad\quad \bar{u}=0, \qquad \bar{T}=\bar{T}_\infty, \ \bar{C}=\bar{C}_\infty \quad \text{at } \bar{y}\to\infty, \ \bar{x}>0,
\end{aligned} \tag{6}$$

where $\bar{T}_w$ and $\bar{C}_w$ are the wall temperature and concentration, respectively.

The dimensionless variables are defined as follows:

$$x=\frac{\bar{x}}{l}, \ \ y=\frac{\bar{y}}{l}, \ \ u=\frac{\bar{u}}{U}, \ \ v=\frac{\bar{v}}{U}, \ \ T=\frac{\bar{T}-\bar{T}_\infty}{\bar{T}_w-\bar{T}_\infty}, \ \ C=\frac{\bar{C}-\bar{C}_\infty}{\bar{C}_w-\bar{C}_\infty}, \ \ t=\frac{U\bar{t}}{l}, \tag{7}$$

where $U=(\rho L^n/k)^{1/n-2}$ and l is a suitable length scale. Substituting the expressions in equation (7) into equations (2)–(5) yields the following dimensionless equations:

$$\frac{\partial u}{\partial x}+\frac{\partial v}{\partial y}=0, \tag{8}$$

$$\begin{aligned}
\frac{\partial u}{\partial t}+u\frac{\partial u}{\partial x}+v\frac{\partial u}{\partial y}&=Gr\,T+Gc\,C+\frac{\partial}{\partial y}\left(\left|\frac{\partial u}{\partial y}\right|^{n-1}\frac{\partial u}{\partial y}\right)\\
&\quad -K|u|^{n-1}u-k_2|u|u,
\end{aligned} \tag{9}$$

$$\frac{\partial T}{\partial t}+u\frac{\partial T}{\partial x}+v\frac{\partial T}{\partial y}=\frac{Pr}{Re}\frac{\partial^2 T}{\partial y^2}+Ec\left|\frac{\partial u}{\partial y}\right|^n\frac{\partial u}{\partial y}, \tag{10}$$

$$\frac{\partial C}{\partial t}+u\frac{\partial C}{\partial x}+v\frac{\partial C}{\partial y}=\frac{1}{Sc\,Re}\frac{\partial^2 C}{\partial y^2}-\gamma C, \tag{11}$$

where $Re=\frac{Ul}{\nu}$ is the Reynold's number, $K=\frac{\varepsilon^n l^{n+1}}{k_1}$ and $k_2=\frac{F\varepsilon^2 l}{k_1^{1/2}}$ are the dimensionless first and second-order resistance due to the presence of the solid matrix, $Ec=\frac{U^2}{C_p(\bar{T}_w-\bar{T}_\infty)}$ is the Eckert number. $Gr=\frac{g\beta_T(\bar{T}_w-\bar{T}_\infty)l}{U^2}$, $Gc=\frac{g\beta_C(\bar{C}_w-\bar{C}_\infty)l}{U^2}$ are the Grashof number and the modified Grashof number, respectively, $Pr=\frac{\rho\nu C_p}{k}$ is the Prandtl number, $Sc=\frac{\nu}{D}$ is the Schmidt number and $\gamma=\frac{k_c l}{U}$ is the chemical reaction parameter.

The dimensionless initial and boundary conditions become

$$\begin{aligned}
&t=0: \quad u=v=0, \ T=C=0, \quad \text{for all } x \text{ and } y,\\
&t>0: \quad u=v=0, \ T=C=0, \quad \text{at } x=0,\\
&\qquad u=v=0, \ T=C=1 \quad \text{at } y=0, \ x>0,\\
&\qquad u=0, \qquad T=C=0 \quad \text{at } y\to\infty, \ x>0,
\end{aligned} \tag{12}$$

Of special significance for this type of flow and heat and mass transfer situation are the skin-friction coefficient C_f, the Nusselt number Nu and the Sherwood number Sh.

These physical quantities are defined in dimensionless form, respectively, as follows:

$$C_f\, Re^{1/2} = \left|u'(t,x,0)\right|^n, \tag{13}$$

$$Nu\, Re^{-1/2} = -T'(t,x,0), \tag{14}$$

$$Sh\, Re^{-1/2} = -C'(t,x,0). \tag{15}$$

3 Solution technique

The unsteady non-linear coupled equations (8)–(11) subject to the initial and boundary conditions (12) are solved by using an explicit finite-difference scheme. The steady-state condition is assumed to exist when $\partial u/\partial t$, $\partial T/\partial t$ and $\partial C/\partial t$ approach zero in the unsteady-state problem. We assumed that the length of the plate is $X_{max} = 10$ units and the boundary-layer thickness is $Y_{max} = 30$ units. Let u', v', T' and C' denote the values of u, v, T and C at the end of time step. The approximate set of the finite-difference equations corresponding to equations (8)–(11) are:

$$\frac{u'_{i,j} - u'_{i-1,j}}{\Delta x} + \frac{v'_{i,j} - v'_{i-1,j}}{\Delta y} = 0, \tag{16}$$

$$\begin{aligned}
&\frac{u'_{i,j} - u_{i,j}}{\Delta t} + u_{i,j}\frac{u_{i,j} - u_{i-1,j}}{\Delta x} + v_{i,j}\frac{u_{i,j+1} - u_{i,j}}{\Delta y} \\
&\quad = Gr\, T'_{i,j} + Gc\, C'_{i,j} + \left\{ \left| \frac{u_{i,j+1} - u_{i,j}}{\Delta y} \right|^{n-1} \left(\frac{u_{i,j+1} - u_{i,j}}{\Delta y} \right) \right. \\
&\qquad\qquad \left. - \left| \frac{u_{i,j} - u_{i,j-1}}{\Delta y} \right|^{n-1} \left(\frac{u_{i,j} - u_{i,j-1}}{\Delta y} \right) \right\} \Big/ \Delta y \\
&\qquad - K|u_{i,j}|^{n-1} u_{i,j} - k_2 |u_{i,j}| u_{i,j},
\end{aligned} \tag{17}$$

$$\begin{aligned}
&\frac{T'_{i,j} - T_{i,j}}{\Delta t} + u_{i,j}\frac{T_{i,j} - T_{i-1,j}}{\Delta x} + v_{i,j}\frac{T_{i,j+1} - T_{i,j}}{\Delta y} \\
&\quad = \frac{Pr}{Re}\left(\frac{T_{i,j+1} - 2T_{i,j} + T_{i,j-1}}{(\Delta y)^2} \right) \\
&\qquad + Ec \left\{ \left| \frac{u_{i,j+1} - u_{i,j}}{\Delta y} \right|^{n} \left(\frac{u_{i,j+1} - u_{i,j}}{\Delta y} \right) \right. \\
&\qquad\qquad \left. - \left| \frac{u_{i,j} - u_{i,j-1}}{\Delta y} \right|^{n} \left(\frac{u_{i,j} - u_{i,j-1}}{\Delta y} \right) \right\} \Big/ \Delta y,
\end{aligned} \tag{18}$$

$$\begin{aligned}
&\frac{C'_{i,j} - C_{i,j}}{\Delta t} + u_{i,j}\frac{C_{i,j} - C_{i-1,j}}{\Delta x} + v_{i,j}\frac{C_{i,j+1} - C_{i,j}}{\Delta y} \\
&\quad = \frac{1}{Sc\, Re}\left(\frac{C_{i,j+1} - 2C_{i,j} + C_{i,j-1}}{(\Delta y)^2} \right) - \gamma C'_{ij},
\end{aligned} \tag{19}$$

where (i, j) represents the grid points. The coefficients $u_{i,j}$ and $v_{i,j}$ are treated as constants, during any one time-step. Then, at the end of any time step Δt, the new velocity components u' and v', the new temperature T' and the new concentration C' at all interior grid points may be obtained by successive applications of equations (16)–(19). The velocity, temperature and concentration profiles were calculated at various dimensionless times. The region of integration is considered as a rectangle with sides x, $x_{max} = 10$ and y, $y_{max} = 30$ where y_{max} corresponds to $y = \infty$ which lies very well outside the momentum, thermal and concentration boundary layers. After performing few tests on sets of mesh sizes to access grid independence, the time and spatial step sizes $\Delta t = 0.001$, $\Delta x = 1$ and $\Delta y = 1$ were found to give accurate results. The results are presented in the next section with a view to isolate the effect of each individual parameter. The complete results for $t > 20$ show no changes in u, v, T and C. Therefore, the value $t = 20$ is used in most of the figures and is considered as representing the steady-state condition.

4 Results and discussion

In this section, a representative set of graphical steady-state results at $x = 10$ is presented in Figs. 1–20. These figures illustrate the influence of the chemical reaction parameter γ, the modified Grashof number Gc, the Eckert number Ec the Prandtl number Pr, the Schmidt number Sc, the permeability parameter K and the flow process dimensionless time on the steady-state velocity, temperature and the concentration profiles. Some temporal or time-dependent results are shown in Figs. 21–23.

Figs. 1–3 show the influence of the chemical reaction parameter γ on the velocity, temperature and concentration profiles in the boundary layer, respectively. Increasing the chemical reaction parameter produces a decrease in the species concentration. In turn, this causes the concentration buoyancy effects to decrease as γ increases. Consequently, less flow is induced along the plate resulting in decreases in the fluid velocity in the boundary layer. In addition, the concentration boundary layer thickness decreases as γ increases. On the other hand, increasing the chemical reaction parameter produces an increase on the temperature profiles. It should be noted here that for generative chemical reactions ($\gamma < 0$), distinctive peaks in the concentration profiles and change in the sign of their wall slopes occur. This enhances the distinctive peak appearing in the velocity profiles due to the solutal buoyancy effects. These behaviors are clearly evident in Figs. 1–3.

Figs. 4–6 display the effects the modified Grashof number Gc on the velocity, temperature and concentration profiles in the boundary layer for two values of $k_2 = 0, 0.1$, respectively. Increasing the Modified Grashof number Gc leads to an increase in the velocity profiles while it substantially reduces the concentration profile values so that increasing buoyancy body force has an inhibiting effect on the value of contaminant concentration throughout the boundary layer regime normal to the barrier. Also, the temperature profile values are decreased due increases in Gc. In addition, the effects of the local Forchheimer number of porous media $k_2 = 0, 0.1$ are shown clearly shown in Figs. 4–6. As k_2 increases, the flow resistance increases causing the velocity to decrease and the temperature to increase with slight changes in the concentration profiles.

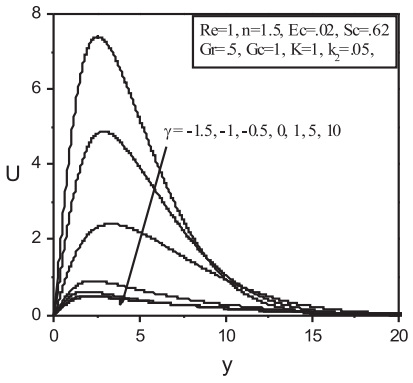

Fig. 1. Effects of the chemical reaction parameter on the velocity profiles.

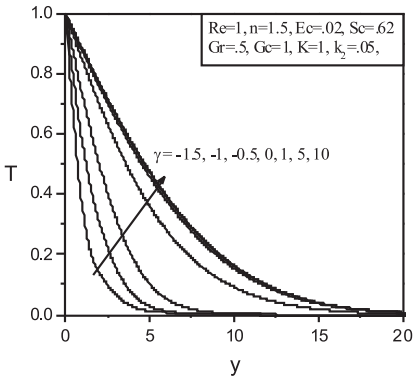

Fig. 2. Effects of the chemical reaction parameter on the temperature profiles.

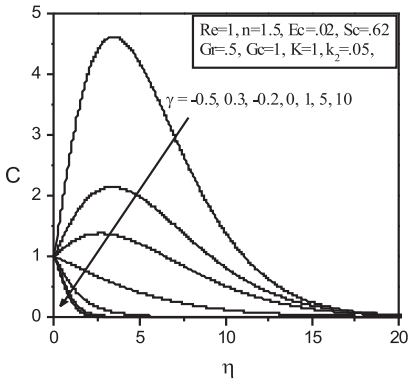

Fig. 3. Effects of the chemical reaction parameter on the concentration profiles.

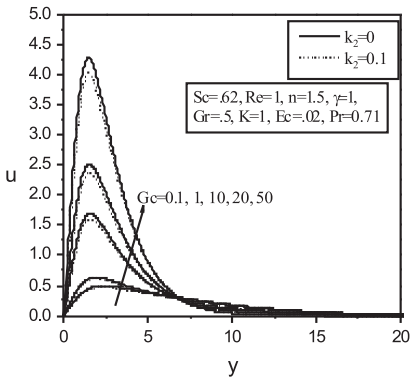

Fig. 4. Effects of the modified Grashof number on the velocity profiles.

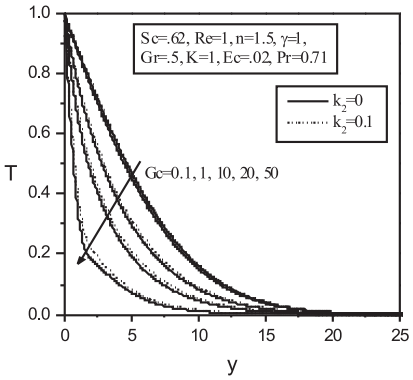

Fig. 5. Effects of the modified Grashof number on the temperature profiles.

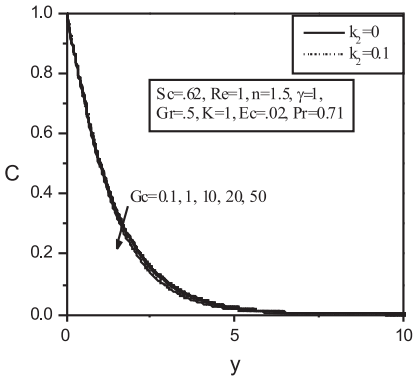

Fig. 6. Effects of the modified Grashof number on the concentration profiles.

Figs. 7 and 8 display the effects of the Eckert number on the velocity and temperature profiles. For the parametric values used to obtain these figures, it is seen that increasing the Eckert number Ec leads to decreases in both the velocity and temperature profiles with no changes in the momentum and thermal boundary layer thicknesses.

Figs. 9 and 10 present the velocity and temperature profiles in the boundary layer for different values of the Prandtl number Pr with two values of $n = 0.5, 1.5$. It is known that the Prandtl number characterizes the ratio of thicknesses of the viscous and thermal boundary layers. Increases in the values of Pr cause the velocity, fluid temperature and the thermal boundary layer thickness to decrease significantly as seen from Figs. 9 and 10.

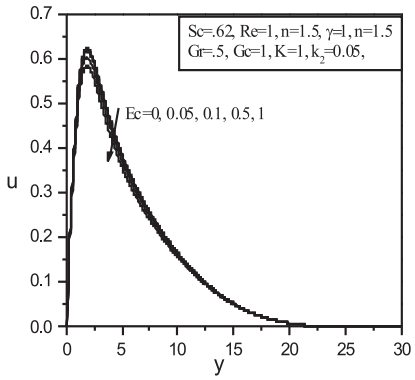

Fig. 7. Effects of the Eckert number on the velocity profiles.

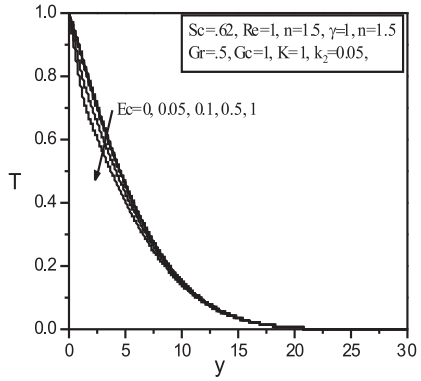

Fig. 8. Effects of the Eckert number on the temperature profiles.

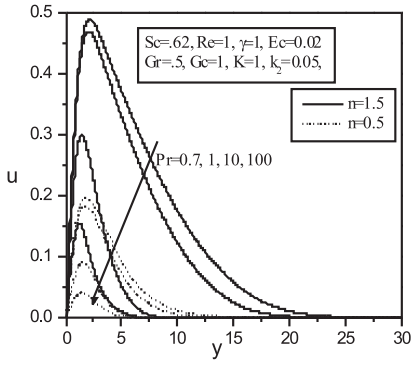

Fig. 9. Effects of the Prandtl number on the velocity profiles.

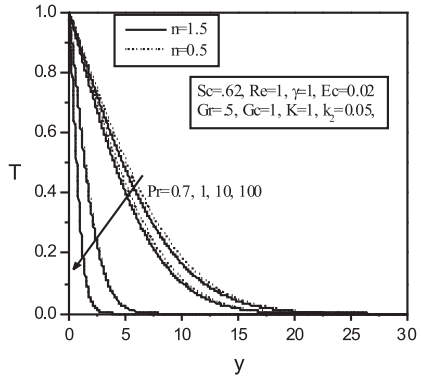

Fig. 10. Effects of the Prandtl number on the temperature profiles.

The effects of increasing the Schmidt number Sc on the velocity, temperature and concentration profiles in the boundary layer are shown in Figs. 11–13. The Schmidt number is an important parameter in heat and mass transfer processes as it characterizes

the ratio of thicknesses of the viscous and concentration boundary layers. Its effect on the species concentration has similarities to the Prandtl number effect on the temperature. That is, increases in the values of Sc cause the velocity and species concentration and its boundary layer thickness to decrease significantly as seen from Figs. 11 and 13. Also, as the Schmidt number increases, the value of fluid temperature increases as seen from Fig. 12.

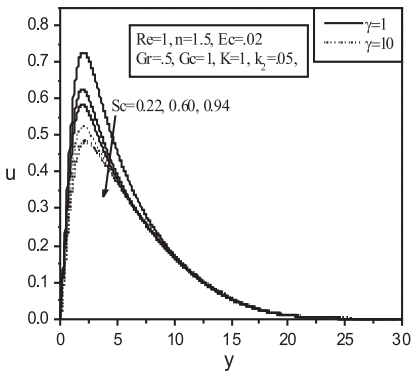

Fig. 11. Effects of the Schmidt number on the velocity profiles.

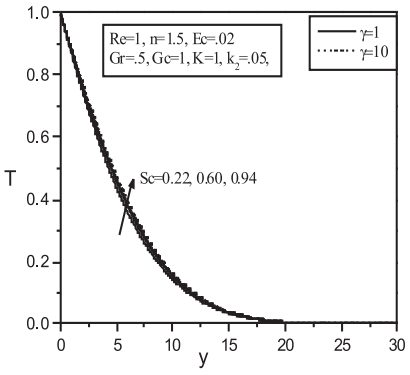

Fig. 12. Effects of the Schmidt number on the temperature profiles.

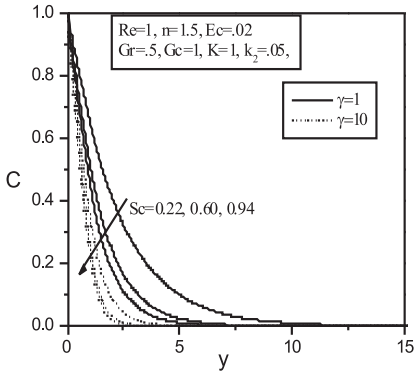

Fig. 13. Effects of the Schmidt number on the concentration profiles.

Figs. 14 and 15 present typical velocity and temperature profiles in the boundary layer for various values of the permeability parameter K, respectively. Increasing the value of K has the tendency to increase the resistance to the flow causing the fluid velocity to decrease and its temperature to increase. This occurs with slight changes in the thicknesses of the momentum and thermal boundary layers.

Figs. 16 and 17 show the velocity and temperature profiles for various values of the power-law fluid index n, respectively. It is clear from these figures that as the power-law fluid index n increases, the fluid velocity u increases significantly while the fluid

temperature T decreases slightly. In addition, while the momentum boundary layer thickness increases as n increases, then thermal boundary layer thickness remains almost unchanged.

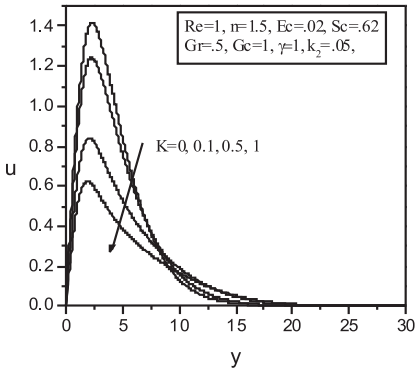

Fig. 14. Effects of the permeability parameter on the velocity profiles.

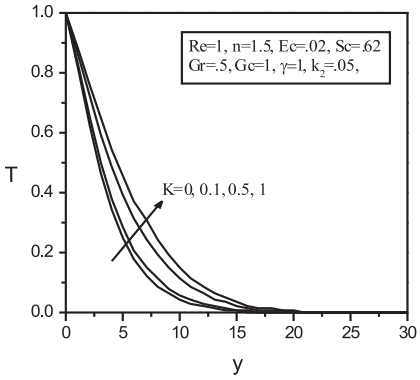

Fig. 15. Effects of the permeability parameter on the temperature profiles.

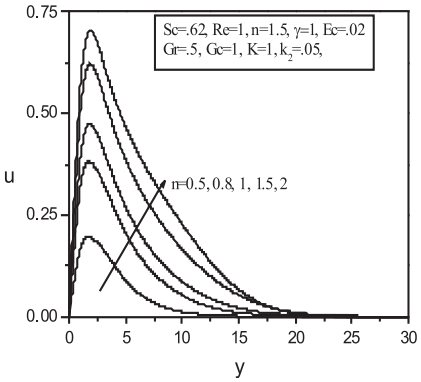

Fig. 16. Velocity profiles for various values of n.

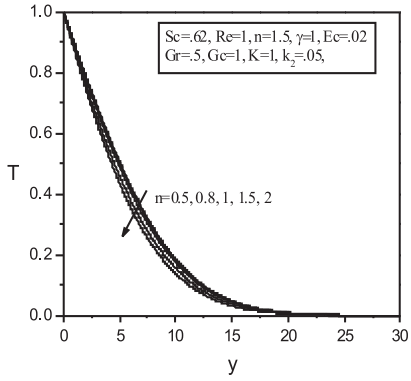

Fig. 17. Temperature profiles for various values of n.

Figs. 18–20 present typical velocity, temperature and concentration profiles in the boundary layer for various values of the axial distance x, respectively. As expected, it is observed that all of the velocity, temperature and concentration increase as x increases.

Figs. 21–23 illustrate the development of the velocity, temperature and concentration profiles in the boundary layer as they develop from the transient state conditions to the steady-state conditions for two values of power-law fluid index n, respectively. It is clearly observed from these figures that that all of the velocity, temperature and concentration increase as time progresses from the transient to the steady-state conditions. For the parametric values used to produce the figures, it is also seen that while it takes longer for the temperature profiles to reach the steady-state conditions, the velocity and the concentration profiles reach these conditions faster.

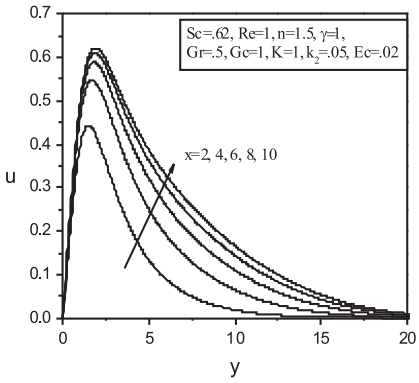

Fig. 18. Velocity profiles for various values of x.

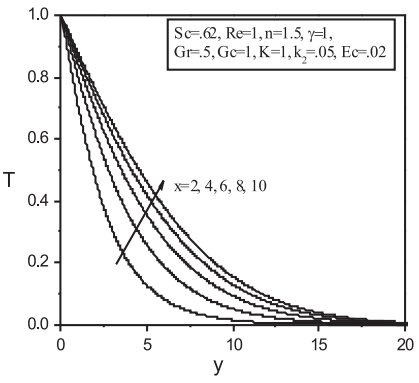

Fig. 19. Temperature profiles for various values of x.

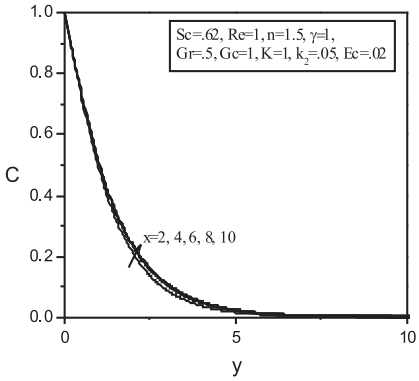

Fig. 20. Concentration profiles for various values of x.

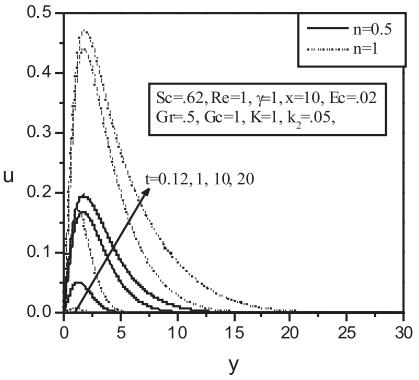

Fig. 21. Development of velocity profiles with time.

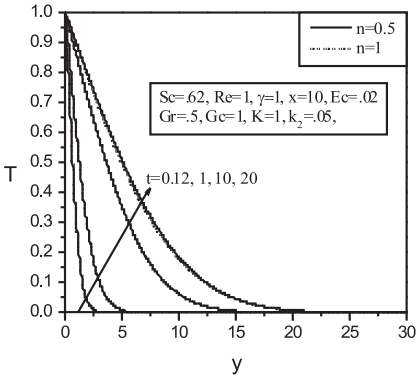

Fig. 22. Development of temperature profiles with time.

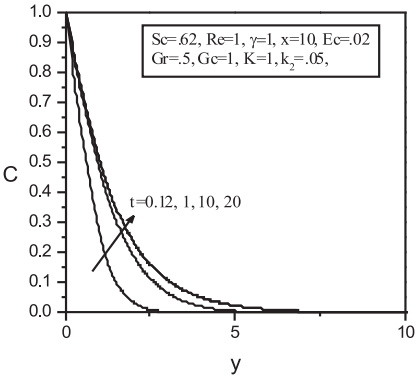

Fig. 23. Development of concentration profiles with time.

Table 1 depicts the effects of power low index n and dimensionless time t on the skin-friction coefficient $(u'(t,x,0))^n$, and the rate of heat and mass transfer $-T'(t,x,0)$ and $-C'(t,x,0)$. It is clearly observed from this table that while the skin-friction coefficient increases as the dimensionless time increases, the rates of heat and mass transfer decrease until they reach the steady state conditions at $t = 20$. It is also seen that the rate of mass transfer reaches steady state at a faster pace than the skin friction and the rate of heat transfer. In addition, it is observed that as the power-law fluid index increases, the rate of heat transfer increases. Also, the rate of mass transfer appears to increase insignificantly as n increases. On the other hand, the skin-friction coefficient is observed to decrease as n increases for $t \leq 1$ while it increases as n is increased from 0.5 to 1 and then decreases as n is increased from 1 to 1.5 for $t = 10$ and $t = 20$.

Table 1. Transient values of $(u'(t,x,0))^n$, $-T'(t,x,0)$ and $-C'(t,x,0)$ for various values of power-law fluid index n and $Gr = 0.5$, $Gc = 1$, $\gamma = 1$, $k_2 = 0.05$, $K = 1$, $Pr = 0.71$, $Sc = 0.62$, $Ec = 0.02$, $Re = 1$ and $x = 10$.

n	t	$(u'(t,x,0))^n$	$-T'(t,x,0)$	$-C'(t,x,0)$
0.5	0.12	0.0604345	0.85580	0.84724
	1	0.2523674	0.44449	0.56948
	10	0.4166372	0.15052	0.53623
	20	0.4455831	0.10726	0.53623
1	0.12	0.0129732	0.85580	0.84724
	1	0.2187688	0.44465	0.56948
	10	0.4419633	0.15228	0.53628
	20	0.4605191	0.11449	0.53651
1.5	0.12	0.0017325	0.85580	0.84724
	1	0.1815046	0.44468	0.56948
	10	0.4385045	0.15419	0.53635
	20	0.4489330	0.12426	0.53660

Table 2 illustrates the influence of the dimensionless first and second-order resistance parameters (permeability and Forchheimer parameters) due to the presence of the solid matrix, (K, k_2) and the values of x on the skin-friction coefficient $(u'(t,x,0))^n$, the rate of heat transfer $-T'(t,x,0)$ and the rate of mass transfer $-C'(t,x,0)$. It is observed that the local skin friction and heat and mass transfer rates decrease due to increases in either of the permeability parameter K or the Forchheimer number of porous media k_2. In addition, as the axial distance x is increased, the skin friction coefficient increased while both rates of heat and mass transfer decreased.

Table 3 illustrates the influence of the solutal buoyancy (modified Grashof number) Gc, the Eckert number Ec and the chemical reaction parameter γ and dimensionless time t on the skin-friction coefficient $(u'(t,x,0))^n$, the rate of heat transfer $-T'(t,x,0)$ and the rate of mass transfer $-C'(t,x,0)$. It is predicted that both the skin-friction coefficient and the Nusselt number increase due to increases in the solutal buoyancy parameter while the skin-friction coefficient decreases as the chemical reaction parameter increases. Also, the

Sherwood number is predicted to increase as either of the solutal buoyancy parameter or the chemical reaction parameter increases. In addition, increasing the Eckert number Ec leads to decreases in both of the local skin-friction coefficient and the Sherwood number while the Nusselt number increases.

Table 2. Transient values of $(u'(t,x,0))^n$, $-T'(t,x,0)$ and $-C'(t,x,0)$ for various values at $Gr = 0.5$, $Gc = 1$, $\gamma = 1$, $n = 1.5$, $Ec = 0.02$, $Pr = 0.71$, $Sc = 0.62$ and $Re = 1$.

k_2	K	x	$(u'(t,x,0))^n$	$-T'(t,x,0)$	$-C'(t,x,0)$
0.0	1	1	0.2251381	0.4574103	0.6178843
		5	0.4344240	0.1812706	0.5387990
		10	0.4582770	0.1252812	0.5366324
0.1		1	0.2214940	0.4554741	0.6171651
		5	0.4192027	0.1781743	0.5385851
		10	0.4401636	0.1232985	0.5365802
1		1	0.1944212	0.4400935	0.6115872
		5	0.3267412	0.1588219	0.5375974
		10	0.3362875	0.1138784	0.5363652
0.05	0.0		1.0764600	0.1999931	0.5400455
	0.1		0.9299890	0.1846139	0.5389129
	0.5		0.6170719	0.1456740	0.5371360
	1		0.4489330	0.1242600	0.5366038

Table 3. Transient values of $(u'(t,x,0))^n$, $-T'(t,x,0)$ and $-C'(t,x,0)$ for various values at $Gr = 0.5$, $k_2 = 0.05$, $K = 1$, $n = 1.5$, $Pr = 0.71$, $Sc = 0.62$, $Re = 1$ and $x = 10$.

Gc	Ec	γ	t	$(u'(t,x,0))^n$	$-T'(t,x,0)$	$-C'(t,x,0)$
1	0.02	-0.5	0.12	0.0018378	0.8558020	0.8337253
			20	18.618.683	0.2766084	$-19.418.221$
		0.0	0.12	0.0018014	0.855802	0.8384073
			20	0.6638802	0.1559451	0.1392612
		1	0.12	0.0017325	0.855802	0.8472365
			20	0.448933	0.124260	0.5366038
		5	0.12	0.0015005	0.855802	0.8764781
			20	0.3232785	0.117435	0.7957801
	0.0	1	20	0.5366068	0.1211106	0.4497317
	0.04			0.5366008	0.1273919	0.4481385
	0.1			0.536592	0.1366847	0.4457806
	0.5			0.5365391	0.194976	0.4309714
	1			0.5364855	0.2600405	0.4144020
0	0.02			0.5365051	0.1150117	0.2337292
0.5				0.536559	0.1194581	0.3411185
1				0.5366038	0.1242600	0.448933
4				0.5369158	0.1578797	1.101.666

Table 4 depicts the effects of the Reynolds number Re, Prandtl number Pr and the Schmidt number Sc on the skin-friction coefficient $((u'(t,x,0))^n$, and the rates of heat and mass transfer $-T'(t,x,0)$ and $-C'(t,x,0)$. It is clearly observed from this table that the skin-friction coefficient decreases as either of the Prandtl number, Reynolds number or the Schmidt number increases. Also, the rate of heat transfer or Nusselt number is predicted to increase due to increases in the Prandtl number while it decreases as either of the Schmidt number and the Reynolds number increases. In addition, the Sherwood number is predicted to increase as a result of increasing either of the Schmidt number, Reynolds number and the Prandtl number.

Table 4. Transient values of $(u'(t,x,0))^n$, $-T'(t,x,0)$ and $-C'(t,x,0)$ for various values at $Gr = 0.5$, $Gc = 1$, $\gamma = 1$, $k_2 = 0.05$, $K = 1$, $Ec = 0.02$, $n = 1.5$, $Sc = 0.62$, $Pr = 0.71$ and $x = 10$.

Re	Sc	Pr	$(u'(t,x,0))^n$	$-T'(t,x,0)$	$-C'(t,x,0)$
1	0.62	0.3	0.4641619	0.0796328	0.5364884
		0.71	0.4492361	0.1233548	0.5366017
		1	0.4410405	0.1481507	0.5366537
		10	0.3552927	0.4437785	0.5367959
	0.22	0.71	0.5352618	0.1327810	0.3722014
	0.60		0.4517598	0.1244743	0.5310420
	0.94		0.4132675	0.1218395	0.6077896
0.1	0.62		0.5317547	0.4384755	0.2201933
1			0.4489330	0.1242600	0.5366038
2			0.4021735	0.0849398	0.6547549
4			0.3578234	0.0592856	0.7645361

5 Conclusions

The problem of unsteady, laminar, heat and mass transfer by natural convection boundary-layer flow of a viscous fluid over a vertical plate to non-Newtonian fluids embedded in a uniform porous medium in the presence of viscous dissipation and first-order chemical reaction effects was considered. Both the wall temperature and wall concentration were assumed to be constant. The governing equations for this problem were developed and non-dimensionalized and the resulting equations were then solved numerically by an explicit finite-difference scheme. It was found that, in general, the skin-friction coefficient increased as the solutal buoyancy, increased and it decreased as a result of increasing either of the local Forchheimer number, permeability parameter, Eckert number, Reynolds number, Prandtl number, Schmidt number or the chemical reaction parameter. In addition, the Nusselt number was predicted to increase due to increases in either of the Prandtl number, solutal buoyancy or the Eckert number while it decreased as either of the local Forchheimer number, permeability parameter, chemical reaction parameter or the Schmidt number increased. Furthermore, the Sherwood number was predicted to

increase as a result of increasing either of solutal buoyancy, Prandtl number, Reynolds number, chemical reaction parameter or the Schmidt number while it decreased as a result of increasing either of the Eckert number, the local Forchheimer number, permeability parameter increased. The skin-friction coefficient increased while the Nusselt number and the Sherwood number decreased as either of the axial distance along the plate or the dimensionless time increased. Finally, it was observed that as the power-law fluid index increased, both rates of heat and mass transfer increased. On the other hand, the skin-friction coefficient was observed to decrease as n increased at small times while it increases as n was increased from pseudo-plastic to Newtonian fluids conditions and then decreased as n was increased from Newtonian to dilitant fluid conditions at large times.

References

1. R. Kandasamy, K. Periasamy, K.K. Sivagnana Prabhu, Chemical reaction, heat and mass transfer on MHD flow over a vertical stretching surface with heat source and thermal stratification effects, *Int. J. Heat Mass Tran.*, **48**, pp. 4557–4561, 2005.

2. J.D. Goddard, A. Acrivos, An analysis of laminar forced-convection mass transfer with homogeneous chemical reaction, *Q. J. Mech. Appl. Math.*, **20**, pp. 473–496, 1967.

3. B. Gebhart, *Heat Transfer*, 2nd ed., McGraw Hill Inc., New York, 1971.

4. U.N. Das, R. Deka, V.M. Soundalgekar, Effects of mass transfer on flow past an impulsively started infinite vertical plate with constant heat flux and chemical reaction, *Forsch. Ingenieurwes.*, **60**, pp. 284–287, 1994.

5. K.I. Andersson, O.R. Hansen, and B. Holmedal, Diffusion of a chemically reactive species from a stretching sheet, *Int. J. Heat Mass Tran.*, **37**, pp. 659–664, 1994.

6. M.A. Abd El-Naby, E.M.E. Elbarbary, N.Y. Abed Elazem, Finite difference solution of radiation effects on MHD unsteady free-convection flow over vertical porous plate, *Appl. Math. Comput.*, **151**, pp. 327–346, 2004.

7. P. Ganesan, G. Palani, Finite difference analysis of unsteady natural convection MHD flow past an inclined plate with variable surface heat and mass flux, *Int. J. Heat Mass Tran.*, **47**, pp. 4449–4457, 2004.

8. S.M.M. EL-Kabeir, A.M. Rashad, R.S.R. Gorla, Unsteady MHD combined convection over a moving vertical sheet in a fluid saturated porous medium with uniform surface heat flux, *Math. Comput. Model.* **46**, pp. 384–397, 2007.

9. I.U. Mbeledogu, A. Ogulu, Heat and mass transfer of an unsteady MHD natural convection flow of a rotating fluid past a vertical porous flat plate in the presence of radiative heat transfer, *Int. J. Heat Mass Tran.*, **50**, pp. 1902–1908, 2007.

10. R. Usha, R. Sridharan, On the motion of a liquid film on an unsteady stretching surface, *J. Fluid. Eng.-T. ASME*, **150**, pp. 43–48, 1993.

11. H.I. Andersson, J.B. Aareth, B.S. Dandapat, Heat transfer in a liquid film on an unsteady stretching surface, *Int. J. Heat Mass Tran.*, **43**, pp. 69–74, 2000.

12. H.I. Andersson, J.B. Aareth, N. Braud, B.S. Dandapat, Flow of a power-law fluid film on an unsteady stretching surface, *J. Non-Newton. Fluid*, **62**, pp. 1–8, 1996.

13. C.-H. Chen, Heat transfer in a power-law fluid film over a unsteady stretching sheet, *Heat Mass Transfer*, **39**, pp. 791–796, 2003.

14. A. Alizadeh-Pahlavan, K. Sadeghy, On the use of homotopy analysis method for solving unsteady MHD flow of Maxwellian fluids above impulsively stretching sheets, *Commun. Nonlinear Sci.*, **14**, pp. 1355–1365, 2009.

15. O.A. Bég, J. Zueco, T.A. Bég, H.S. Takhar, E. Kahya, NSM analysis of time-dependent nonlinear buoyancy-driven double-diffusive radiative convection flow in non-Darcy geological porous media, *Acta Mech.*, **202**, pp. 181–204, 2009.

16. B. Vujanovic, A.M. Stauss, Dj. Djukic, A variational solution of the Rayleigh problem for a power law non-Newtonian conducting fluid, *Ing. Arch.*, **41**, pp. 381–386, 1972.